

AD 744702

ARL 72-0025  
MARCH 1972



## **Aerospace Research Laboratories**

### **HEAT TRANSFER AND ATTRITION PROCESSES AT THE ANODE OF PULSED HIGH INTENSITY ARCS**

*J. L. SMITH*

*E. PFENDER*

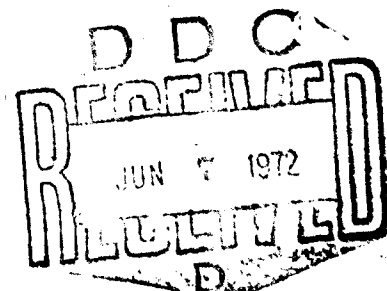
*E. R. G. ECKERT*

*UNIVERSITY OF MINNESOTA,  
MINNEAPOLIS, MINNESOTA*

Details of illustrations in  
this document may be better  
studied on microfiche

CONTRACT NO. F33615-70-C-1668  
PROJECT NO. 7063

Approved for public release; distribution unlimited.



**AIR FORCE SYSTEMS COMMAND**

**United States Air Force**

Reproduced by  
NATIONAL TECHNICAL  
INFORMATION SERVICE  
U S Department of Commerce  
Springfield VA 22151

ARL 72-0025

**HEAT TRANSFER AND ATTRITION  
PROCESSES AT THE ANODE  
OF PULSED HIGH INTENSITY ARCS**

*J. L. SMITH, L. J. LENDER, AND E. R. G. ECKERT*

*HEAT TRANSFER DIVISION  
DEPARTMENT OF MECHANICAL ENGINEERING  
UNIVERSITY OF MINNESOTA  
MINNEAPOLIS, MINNESOTA*

MARCH, 1972

CONTRACT F33615-70-C-1668  
PROJECT 7063

Approved for public release; distribution unlimited.

AEROSPACE RESEARCH LABORATORIES  
AIR FORCE SYSTEMS COMMAND  
UNITED STATES AIR FORCE  
WRIGHT-PATTERSON AIR FORCE BASE, OHIO

## FOREWORD

This final report was prepared by the Department of Mechanical Engineering, University of Minnesota, and covers work performed during the period from June 16, 1970, to December 15, 1971, under Contract F 33615-70-C-1668 for the Aerospace Research Laboratories, Air Force Systems Command, USAF. The actually funded contracting period was from June 16, 1970, to June 15, 1971.

The research reported herein was accomplished on Project 7063 under the technical cognizance of Mr. K. R. Cramer of the Thermomechanics Research Laboratory, ARL.

ACCESSION TO:	
CFSTI	WHITE SECTION
DDC	BLUE SECTION <input type="checkbox"/>
CHAN. CED.	<input type="checkbox"/>
JUSTIFICATION	
BY	
DISTRIBUTION/AVAILABILITY	
DIST.	AVAIL.
A	

# NOTICES

Government drawings, specifications, or other data are used for any purpose other than in connection with a definitely related Government procurement operation, the United States Government thereby incurs no responsibility nor any obligation whatsoever; and the fact that the Government may have formulated, furnished, or in any way supplied the said drawings, specifications, or other data, is not to be regarded by implication or otherwise as in any manner licensing the holder or any other person or corporation, or conveying any rights or permission to manufacture, use, or sell any patented invention that may in any way be related thereto.

Agencies of the Department of Defense, qualified contractors and other government agencies may obtain copies from the

Defense Documentation Center  
Cameron Station  
Alexandria, Virginia 22314

This document has been released to the

CLEARINGHOUSE  
U. S. Department of Commerce  
Springfield, Virginia 22151

for sale to the public.

Copies of ARL Technical Documentary Reports should not be returned to Aerospace Research Laboratories unless return is required by security considerations, contractual obligations or notices on a specified document.

AIR FORCE: 23-572/400

UNCLASSIFIED

DOCUMENT CONTROL DATA - R & D		
(Security classification of title, body of abstract and index of annotation must be entered when the overall report is classified)		
1. ORIGINATING ACTIVITY (Corporate author) University of Minnesota Department of Mechanical Engineering Minneapolis, Minnesota 55445		2. REPORT SECURITY CLASSIFICATION UNCLASSIFIED
3. REPORT TITLE Heat Transfer and Attrition Processes at the Anode of Pulsed High Intensity Arcs		
4. DESCRIPTIVE NOTES (Type of report and inclusive dates) Scientific - Final		
5. AUTHOR(S) (Last name, middle initial, first name) J. L. Smith E. Pfender E. R. G. Eckert		
6. REPORT DATE March 1972	7a. TOTAL NO. OF PAGES 50	7b. NO. OF REFS 12
8a. CONTRACT OR GRANT NO. F33615-70-C-1668		9a. ORIGINATOR'S REPORT NUMBER(S)
b. PROJECT NO. 7063-00-13		9b. OTHER REPORT NO(S) (Any other numbers that may be assigned this report) ARL 72-0025
c. DoD Element 61102F		
d. DoD Subelement 681307		
10. DISTRIBUTION STATEMENT Approved for public release; distribution unlimited.		
11. SUPPLEMENTARY NOTES TECH OTHER		12. SPONSORING MILITARY ACTIVITY Acrospace Research Laboratories (LV) Wright-Patterson AFB, Ohio 45433
13. ABSTRACT Tests of a high current pulsed arc with the intent to investigate anode erosion characteristics are described. The range of arc parameters covers currents from 5000 to 10,000 amps (square pulse) with time intervals from $20 \times 10^{-6}$ to $200 \times 10^{-6}$ seconds. The arc is designed to be stationary; i.e., there are no external magnetic fields and the arc configuration produces self-magnetic fields which are symmetric so as not to move it. It is found, however, that with any but flat electrodes there is an inherent self-magnetic field which will move the attachment points for sufficiently high currents. Spectrometric investigations reveal that there is no anode vaporization for the range of parameters investigated. Rather liquid metal is generated and blown by the action of cathode jet in a radial direction maintaining a relatively cool surface. The cathode, on the other hand, vaporizes in a matter of a few tens of a microsecond for an arc of a few hundred amps. A computer program is described for solving the one-dimensional problem of a constant heat flux impinging on a surface of a material with temperature dependent properties with a liquid-solid interface penetrating the material.		

DD FORM 1 NOV 65 1473

UNCLASSIFIED

Security Classification

A

Electrode Attrition  
Anode  
Arcs  
Pulsed

## ABSTRACT

Tests of a high current pulsed arc with the intent to investigate anode erosion characteristics are described.

The range of arc parameters covers currents from 5000 to 10,000 amps (square pulse) with time intervals from  $20 \times 10^{-6}$  to  $200 \times 10^{-6}$  seconds.

The arc is designed to be stationary; i.e., there are no external magnetic fields and the arc configuration produces self-magnetic fields which are symmetric so as not to move it. It is found, however, that with any but flat electrodes there is an inherent self-magnetic field which will move the attachment points for sufficiently high currents.

Spectrometric investigations reveal that there is no anode vaporization for the range of parameters investigated. Rather liquid metal is generated and blown by the action of cathode jet in a radial direction maintaining a relatively cool surface.

The cathode, on the other hand, vaporizes in a matter of a few tens of microsecond for an arc of a few hundred amps.

A computer program is described for solving the one-dimensional problem of a constant heat flux impinging on a surface of a material with temperature dependent properties with a liquid-solid interface penetrating the material.

## TABLE OF CONTENTS

SECTION	PAGE
FOREWORD	ii
ABSTRACT	iii
TABLE OF CONTENTS	iv
NOMENCLATURE	v
LIST OF ILLUSTRATIONS	vii
I. INTRODUCTION	1
II. ANALYTICAL CONSIDERATIONS	3
III. EXPERIMENTS	15
A. Apparatus	15
B. Experimental Procedure	18
C. Results	25
IV. SUMMARY AND CONCLUSIONS	27
V. REFERENCES	28

## NOMENCLATURE

a	=	Arbitrary constant
C	=	Capacitance
c	=	Specific heat
B	=	$\Delta\tau/(\Delta x)^2$
CHI	=	Non-dimensional quantity indicating heat flux, Eq. 10
E	=	Internal energy (energy units/unit volume)
$f_1$	=	Function defined by Eq. 6c
$f_2$	=	Function defined by Eq. 6a
H	=	Front face heat flux
$H_f$	=	Latent heat of fusion
I	=	Current
K	=	Thermal conductivity
L	=	Inductance
N	=	Number of elements in Guillemin network
T	=	Temperature
$T_M$	=	$T_m - T_{\text{Ambient}}$
U	=	Capacitor charging voltage
u	=	Non-dimensional temperature, Eq. 3
w	=	Non-dimensional temperature, corresponds to u, but a solution to the finite difference equation
x	=	Real space variable
Z	=	Impedance
z	=	Non-dimensional space variable, Eq. 7a
$\phi$	=	Function defined by Eq. 6e
$\beta$	=	Coefficient chosen for Eq. 6a

- $\Delta$  = Equal by definition
- $\delta$  = Transmission line transit time
- $\gamma$  = Fraction of first phase
- $\rho$  = Density
- $\tau$  = Non-dimensional time, Eq. 2
- $\lambda$  = Constant defined by Eq. 6d

### Subscripts

- Amb = Ambient
- f = Subscript on H, latent heat of fusion
- i = Refers to space step
- k = Refers to time step
- M = Used only for  $T_M = T_m - T_{Amb}$
- m = Refers to value of variable at the melting point
- o = Properties at temperatures at which  $K_o$  and  $c_o$  are chosen, see Eq. 6b
- V = Vaporization

## LIST OF ILLUSTRATIONS

FIGURE		PAGE
1	Copper Thermal Conductivity	30
2	Specific Heat of Copper	31
3	Dimensionless Temperature ( $u$ ) for Copper	32
4	Copper $\phi(u)$	33
5	Time to Melting and Vaporization	34
6	Guillemin Network	35
7	Current for Guillemin Network Discharging into Resistive Loads	35
8	Anode-Cathode Mounting	36
9	Circuit with Cathode/Sparker	37
10	Circuit with Solid Cathode	37
11	Current and light emission ( $5218 \text{ \AA}$ ) for $N_2$ arc with copper anode; current 4166 Amp/cm, light relative magnitude only; second firing shows current reversal	38
12 - 15	Cathode Designs	39
16 - 19	Cathode Designs	40
20	Cathode Design	41
21	Some Typical Anode Erosion Marks	42

## I. INTRODUCTION

Although electric arcs and transient discharges have been known for many decades, their electrode regimes are still poorly understood. There is, for example, even for steady arcs no consistent quantitative theory of the anode region available which would permit a complete interpretation of the observed anode phenomena.

The physical dimensions of and the extreme conditions in the anode region of high intensity discharges prohibit the application of many conventional diagnostic tools. In addition to the usual problems of probing the fall spaces without disturbing the plasma, one finds severe problems associated with unavoidable erosion as steady state conditions are approached. Measurements in transient discharges of short duration require careful shielding of the electrical circuits in order to reduce the extremely high noise levels superimposed to electric signals.

Any improvement of existing plasma devices, as for example, arc gas heaters, plasma torches for welding, cutting, and spraying, as well as new developments require, however, a thorough understanding of the electrode regions because excessive electrode attrition represents the limiting factor for the lifetime of such devices.

Although numerous attempts have been made to improve our understanding of the electrode regions, available results are frequently concerned only with phenomenological observations and

the interpretation of the results sometimes leads to contradicting conclusions. Since electrode attrition can be reduced by continuously moving the electrode attachments, magnetically driven arcs attracted increasing interest. It is, however, difficult to gain a fundamental understanding of the electrode regions from such experiments because of the unknown effects of the magnetic field on the electrode regions.

The electrode regions of stationary arcs have been studied by a number of investigators (12, 14, 15). Most of them, however, are only concerned with data for a particular application which contribute little to a fundamental understanding.

In order to arrive at conclusions of general validity, undesirable side effects have to be eliminated. A striking example of such a side effect is the cathode jet impinging on the anode surface at the location of the anode arc attachment. The observed anode erosion pattern changes drastically if the influence of the cathode jet is eliminated.

The objective of this study is a quantitative assessment of the heat transfer to and the associated attrition of the anode in a pulsed high intensity arc. The establishment of well defined and reproducible conditions at the anode is a prerequisite for meaningful data and, therefore, this aspect is particularly emphasized.

## II. ANALYTICAL CONSIDERATIONS

### Concepts

One can think of the following sequence of events in the anode when the arc is struck: First, the surface begins to heat up and a temperature profile is established according to the conduction equation for a surface heat flux (neglecting Joule heating) until the surface reaches the melting temperature, at which point a liquid-solid interface begins to penetrate the anode as the surface temperature continues to rise until the surface reaches the vaporization temperature.

The assumptions in the above picture are that Joule heating is negligible with respect to the surface heat flux and that the liquid layer is stationary. The first assumption is considered by Ref. 13. Ref. 14 did an experimental work which essentially investigated this question and concluded volumetric heating does occur in the anode. However, for the same arc it was concluded that volumetric heating did not occur at the cathode. This is obviously self-contradictory, as it is well accepted that the current density is higher at the cathode than at the anode so that, if the current density at the anode is sufficient to cause appreciable Joule heating, there will most certainly also be Joule heating at the cathode. It is much more likely that, as will be discussed later, the anode heats relatively slowly and consequently builds up a relatively thick liquid layer which is then blown out by the cathode jet. Thus, the second critical assumption that the

liquid layer is stationary for this model comes into play. This assumption will likely be good as long as one can eliminate the cathode jet impingement onto the anode surface which, of course, one must do if one is truly to look at anode phenomena. Also, the surface must reach vaporization relatively quickly.

Exactly what relatively quickly is depends on the gas pressures to which the liquid layer is exposed. If the inertia of the material holds it essentially stationary in the time it takes to reach vaporization, then the assumption is good. A priori this seems most likely. If, on the other hand, gas pressure is sufficient to move the liquid layer almost instantaneously, then the model would have to be changed to the assumption that the liquid layer is removed as soon as it is formed and then the heat flux would be deduced from the time to the onset of erosion and/or the depth of the erosion pit for a given duration arc. Which of these is the best assumption cannot be said before the experiment is actually performed. Because the times involved are short and there is no anticipated source of high gas velocities, assuming that the cathode jet influence is removed, one would expect the former to be best. However, the heat flux can be only estimated to within about two orders of magnitude (discussion following Ref. 12 and Fig. 5) and the phenomena in the fall regions are not completely understood, so one cannot say with certainty that the liquid will remain stationary.

### Basic Equations

#### General Problem:

This really represents two problems in one; the first being conduction in a solid, and the second being conduction through a liquid, through a moving liquid solid boundary, then through a solid.

The first part is governed by the equation

$$\frac{\partial T_2}{\partial t} = \alpha_2 \frac{\partial^2 T_2}{\partial x^2}$$

with boundary conditions

$$Q(x=0) = H = \text{Const}$$

$$\lim_{x \rightarrow \infty} \frac{\partial T_2(t, x)}{\partial x} = 0$$

$$\lim_{x \rightarrow \infty} T_2(t, x) = T_{\text{Amb}}$$

and initial condition

$$T(0, x) = T_{\text{Amb}}$$

The second part may be represented by the following equations:

Liquid Region  $\frac{\partial T_1}{\partial t} = \alpha_1 \frac{\partial^2 T_1}{\partial x^2}$

$$\text{Solid Region} \quad \frac{\partial T_2}{\partial t} = \alpha_2 \frac{\partial^2 T_2}{\partial x^2}$$

$$\text{Solid-Liquid Interface} \quad \rho H_f \frac{dX(t)}{dt} = k_1 \frac{\partial T_1}{\partial x} - k_2 \frac{\partial T_2}{\partial x}$$

The following boundary conditions apply to these equations:

$$X(0) = 0$$

$$T_1(t, X(t)) = T_2(t, X(t)) = T_m$$

$$\lim_{x \rightarrow \infty} \frac{\partial T_2(t, x)}{\partial x} = 0$$

$$\lim_{x \rightarrow \infty} T_2(t, x) = T_{\text{Amb}}$$

$T_2(0, x)$  = solution to first problem when the surface reaches the melting temperature

Constant Property Solution:

When material properties are assumed to be independent of temperature, the solution is considerably simplified. The first part of the problem has an analytic solution (Ref. 9).

The time required for the surface to reach melting is

$$t_m = \frac{\pi (T_M)^2 k_2 \rho c_2}{4 H^2}$$

with a corresponding temperature profile of

$$T - T_{\text{Amb}} = T_M \exp\left(-\frac{x^2 H^2}{T_M^2 K_2^2 \pi}\right) - \frac{hx}{K_2} \operatorname{erfc}\left(\frac{xH}{T_M K_2 \sqrt{\pi}}\right)$$

The second part of the problem is exactly as previously stated except that  $T_2(0,x)$  is known. This is one of the many variations of the "Stefan Problem" which has no analytic solution. It is, however, amenable to an analog computer solution and has been solved for a number of metals by Cohen (Ref. 1).

Unfortunately, the constant property assumption is not a good one for most materials.

#### Variable Property Solution:

The moving boundary between the solid and liquid regimes presents a considerable complication as compared to a single phase conduction problem. However, a clever way of circumventing this problem has been developed by Hashemi and Sliepcevich (Ref. 2). Essentially it consists of assuming that melting occurs over a small but finite temperature range, rather than at a particular temperature. This assumption allows one to consider the melting problem as a conduction problem of a single phase with variable properties, as will be seen.

This approximation may be thought of in the following manner. If the material in question melts at a single temperature, the latent heat of fusion can be looked at as an impulse function in the specific heat located at the melting temperature. We

assume this spike is not infinitely narrow but is a pulse of finite width.

If the material is not pure, this assumption is probably more nearly an accurate model of the real situation than would be a single melting point. It provides a very convenient means of accounting for phase transitions which occur in materials such as iron. Phase transitions in these materials appear as fairly wide pulses in the specific heat curves.

The heat conduction equation may be written as

$$\frac{\partial}{\partial x} \left( K \frac{\partial T}{\partial x} \right) = \rho \left( \frac{1}{\rho} \left( \frac{\partial E}{\partial T} \right)_{\rho} \right) \frac{\partial T}{\partial t} \quad (1)$$

Note that specific heat is not used, but rather  $\frac{1}{\rho} \left( \frac{\partial E}{\partial T} \right)_{\rho}$  in anticipation of the use of a fictional specific heat which includes the latent heat of fusion.

Define

$$\tau \triangleq (t/a^2) (H^2/T_M^2 K_0 \rho c_0) \quad (2)$$

$$u \triangleq \int_{T_{\text{Amb}}}^T K dT / \int_{T_{\text{Amb}}}^{T_V} K dT \quad (3)$$

which transforms Equation (1) to

$$\frac{\partial^2 u}{\partial x^2} = \frac{\rho}{K} \left( \frac{1}{\rho} \left( \frac{\partial E}{\partial T} \right)_{\rho} \right) \frac{\partial (u)}{\partial \tau} (H^2/a^2 T_M^2 K_0 \rho c_0) \quad (4)$$

Using the procedure of Ref. 2,

$$\begin{aligned} \frac{1}{\rho} \left( \frac{\partial E}{\partial T} \right)_{\rho} &= c(T) + H_f \left( \frac{\partial \gamma}{\partial T} \right)_{\rho} \\ &= c(T) + H_f \left( \frac{\partial \gamma}{\partial u} \right)_{\rho} \frac{-\frac{K(T)}{\int_{T_{\text{Amb}}}^{T_V} K dT}}{\rho} \end{aligned} \quad (5)$$

Equation (4) then becomes

$$\frac{\partial^2 u}{\partial x^2} = \left( \frac{H}{a T_M K_0} \right)^2 \left( \frac{K_0 c(u)}{c_0 K(u)} + \frac{K_0 H_f \left( \frac{\partial \gamma}{\partial u} \right)_{\rho}}{c_0 \int_{T_{\text{Amb}}}^{T_V} K dT} \right) \frac{\partial u}{\partial \tau} \quad (6)$$

The following definitions and assumptions are made

$$\left( \frac{\partial \gamma}{\partial u} \right)_{\rho} = \frac{\beta}{\sqrt{\pi}} e^{-\beta^2 (u_m - u)^2} \triangleq f_2(u) \quad (6a)$$

Note that as  $\beta \rightarrow \infty$ ,  $f_2$  becomes an impulse function at  $(u_m)$ . Also note that  $\int_{-\infty}^{\infty} f_2(u) du = 1.0$ .

Choose  $u_0$  such that

$$K_0/c_0 = \text{Max}_{0 \leq u \leq 1} (K(u)/c(u)) \quad (6b)$$

$$f_1(u) \triangleq \frac{K_0/c_0}{K(u)/c(u)} - 1.0 \quad (6c)$$

$$\lambda \triangleq H_f / (c_0 \int_{T_{\text{Amb}}}^{T_V} K(T)/K_0 dT) \quad (6d)$$

$$\phi(u) = 1 + f_1(u) + \lambda f_2(u) \quad (6e)$$

With these applied to Equation (6), it becomes

$$\frac{\partial^2 u}{\partial x^2} = \phi(u) \frac{\partial u}{\partial \tau} \left( \frac{H}{a T_M K_0} \right)^2 \quad (7)$$

Define

$$z \triangleq H x / a T_M K_0 \quad \text{Then Equation (7) becomes} \quad (7a)$$

$$\frac{\partial^2 u}{\partial z^2} = \phi(u) \frac{\partial u}{\partial \tau} \quad (8)$$

The function  $\phi(u)$  can be evaluated from a knowledge of material properties.

Using the Crank-Nicholson method, the finite difference form of Equation (8) becomes

$$\begin{aligned} & \phi(w_{i,k+1/2}) \left( \frac{w_{i,k+1} - w_{i,k}}{\Delta \tau} \right) = \\ & = \frac{(w_{i-1,k} - 2w_{i,k} + w_{i+1,k}) + (w_{i-1,k+1} - 2w_{i,k+1} + w_{i+1,k+1})}{2(\Delta z)^2} \end{aligned}$$

where

$i$  refers to position

$k$  refers to time

$w$  is used to denote the solution to the finite difference equation, corresponding to  $u$  which is the solution to the differential equation

Since  $\Delta z$  contains an arbitrary scale factor, we can set

$$\Delta z = 1 \text{ and}$$

$$\Delta \tau / (\Delta z)^2 = B$$

The stability of this equation has been considered (Ref. 3) with the conclusion that it is unconditionally stable. However, it was considered for  $\phi$  evaluated at the  $k^{\text{th}}$  node rather than  $(k+1/2)$ . Douglas (Ref. 4) recommends evaluation at node  $(k+1/2)$  for a general form of Equation (2); it is suggested to evaluate  $\phi$  at  $(k+1/2)$  by an iterative procedure, a backward difference method, or an extrapolation from previous times. The first two of these would cost computer time so the latter is preferable if feasible. In the solution for copper, it was found to matter little whether  $\phi(i,k)$  or  $\phi(i,k+1/2)$  was used. The equations were first solved using  $\phi(i,k)$  and the solution examined to see the feasibility of predicting  $w(i,k+1/2)$  from  $w(i,k)$  and  $w(i,k-1)$ . It was found that except initially at the front face, a linear extrapolation would come quite close. Further, the function  $\phi$  was fortuitously close to constant at low values of  $w$  so that where the linear extrapolation was not valid the error was small.

The boundary conditions to be used in conjunction with Equation (9) in order to obtain the solution are

Front face:

$$H = -K \left( \frac{\partial T}{\partial x} \right)_{x=0} = - \int_{T_{\text{Amb}}}^{T_V} K dT \left( \frac{\partial u}{\partial x} \right)_{x=0}$$

$$\frac{w_{1,k} - w_{2,k}}{\Delta x} = H / \int_{T_{\text{Amb}}}^{T_V} K dT$$

This may be written in terms of ( $\Delta z$ ) and recalling that

$$\Delta z = 1.0$$

$$w_{1,k} - w_{2,k} = \frac{aK_o T_M}{T_v \int_{T_{Amb}} KdT} \triangleq CHI \quad (10)$$

Rear conditions:

$$\frac{\partial u}{\partial x} \Big|_{x \rightarrow \infty} = 0$$

$$w_{I,k} - w_{I-1,k} = 0 \quad \text{for all } k$$

These Equations (4, 5, 6) may be represented in the following matrix form

$$\begin{bmatrix} -1 & 1 & 0 & 0 \\ 1 & -2\left(\frac{\phi_{2,k}}{B} + 1\right) & 1 & 0 \\ 0 & 1 & -2\left(\frac{\phi_{3,k}}{B} + 1\right) & 1 \\ \cdot & \cdot & \cdot & \cdot \\ \cdot & \cdot & \cdot & \cdot \\ \cdot & \cdot & \cdot & \cdot \\ & & \cdot & 1 & 0 \\ & & \cdot & \cdot & \cdot & 1 & -2\left(\frac{\phi_{I-1,k}}{B} + 1\right) & 1 \\ & & \cdot & \cdot & \cdot & 0 & 1 & -1 \end{bmatrix} \begin{bmatrix} w_{1,k+1} \\ w_{2,k+1} \\ \cdot \\ \cdot \\ \cdot \\ \cdot \\ w_{I,k+1} \end{bmatrix} =$$

$$= - \begin{bmatrix} \text{CHI} \\ w_{1,k} + 2 \left( \frac{\phi_{2,k}}{B} - 1 \right) w_{2,k} + w_{3,k} \\ w_{2,k} + 2 \left( \frac{\phi_{3,k}}{B} - 1 \right) w_{3,k} + w_{4,k} \\ . \\ . \\ . \\ w_{I-2,k} + 2 \left( \frac{\phi_{I-1,k}}{B} - 1 \right) w_{I-1,k} + w_{I,k} \\ 0 \end{bmatrix} \quad \text{for all } k$$

In this form, it may be solved successively for each time interval if an initial temperature profile is assumed.

Note that this transformation of variables results in complete elimination of heat flux from the equations. This permits one solution to be applied to any heat flux just as long as the one-dimensional criterion is met.

#### Equations as applied to the solution for copper

The thermal conductivity for copper was taken from Ref. 6. Separate polynomials were fit to the curves for the liquid region and for solid region from which  $u$  was calculated (Fig. 1, 2, and 3). The specific heat was taken from Ref. 5. A polynomial in  $u$  was fit to the curve of  $\frac{C}{K}$  versus  $u$  as calculated from these properties. From this, an equation for  $f_1$  was obtained. To

obtain the value of  $f_2(u)$ , a value of  $\beta = 30$  was taken and  $u_m$  set at the value corresponding to the melting temperature was taken. This gives a  $\phi$  as shown in Fig. 4. In this figure, the actual and assumed curves for  $\phi$  are shown. The actual curve would have an impulse function at  $u = 0.5988$  (melting point of copper) whereas the assumed curve has the spike shown.

The results of the computer program are shown in Fig. 5. Note that the time to vaporization is considerably less than calculated by Cohen [1]. This is very reasonable as the value of the thermal conductivity is much lower in the liquid region than in the solid region. Cohen's calculation used a constant conductivity value equal to the value at room temperature.

### III. EXPERIMENTS

#### A. Apparatus

##### Current Source

A Guillemin line with a matched load and low inductance leads to the test chamber provides a square current pulse of variable duration and magnitude. The Guillemin network is a lumped parameter simulation of a transmission line. As the number of elements increases, it becomes quite a close approximation to a transmission line and all results of transmission line theory are applicable. The basic properties of such a network are examined in Ref. 10 and 11.

The output impedance must be matched to the L-C network according to

$$Z_0 = \sqrt{L/C}$$

If this is the case, the pulse will be square of amplitude

$$I = U/2 Z_0 \quad (\text{See Fig. 7a})$$

The pulse duration is twice the transit time for the simulated transmission line.

$$\text{i.e., } \tau = 2\delta = 2N \sqrt{CL}$$

It turns out that the results shown in Fig. 7b and 7c are extremely important for this application. Note particularly

that in Fig. 7c, characteristic of an undersized output impedance, the circuit has a tendency toward a damped oscillatory current in the load. This, as will be discussed later, is a critical point to observe.

#### Test Chamber and Electrodes

The chamber in which the electrodes are housed is constructed of a 12-inch diameter by 9-inch high by 1-inch thick aluminum cylinder. There are two 5-inch diameter windows located midway vertically and directly opposite each other. A vacuum connection is provided at 90° to each window.

The main electrical leads are through the bottom of the chamber. The anode is located below the cathode, and its connection comes directly up through the center of the lower cover (Fig. 8). The cathode, located on the axis of the chamber above the anode, is mounted in a symmetric manner on two posts from the bottom of the chamber.

The anode samples are in the shape of  $1\frac{1}{4}" \times 1\frac{1}{4}" \times \frac{1}{4}"$  pieces. These slip into a tapered mount which provides good electrical contact as well as expedient insertion and removal.

The cathode configuration, generally found to be of significant influence on the anode, will be discussed extensively later.

#### Matching Resistance/Low Inductance Leads

It is important that, if the ideal characteristic current of Fig. 7a is to be achieved, the output impedance be nearly a

pure resistance. If there is appreciable inductance, the pulse rise time will be slowed. To avoid this, the connection from the Guillemin network is made via a line made of two 4-inch x .001-inch stainless strips separated by .003-inch mylar and clamped together.

The capacitor bank is housed in a specially constructed cabinet 7 ft. long x 4 ft. high x 3 ft. deep. The connections to the bank exit from one end.

This provides a rise time essentially limited only by the L-C values of the Guillemin network.

#### Circuit

There are two basic circuits which have been used. At times a cathode was used which had a sparker to ignite the arc (Fig. 9), whereas in later experiments it was found that the cathode was influencing the anode so cathodes without sparkers were used (Fig. 10).

#### Spectrometer and Instrumentation

A Jarrel Ash Model 82-020 spectrometer is used with an RCA IP28 photomultiplier with a special dynode chain and mount to provide a signal to a Tektronix 555 dual beam oscilloscope. The current shunt and the photomultiplier outputs are simultaneously displayed which provides a time reference for the photomultiplier output.

## B. Experimental Procedure

Two Guillemin networks have been used; the first was a 40 section line of  $1/2$  micro-farad capacitors and  $1/2$  micro-Henry inductors which provided a 40 microsecond pulse of up to 5000 amp and the second a 50 section line of 2 micro-farad capacitors which provides either a 200 microsecond pulse of up to 5000 amps with 2 micro-Henry inductors or a 100 microsecond pulse of up to 10,000 amps with  $1/2$  micro-Henry inductors. The smaller network used a Signalite spark gap and the larger, a Westinghouse 7703 Ignitron as a switch.

### Initial Work

Early experiments used the smaller of the two lines. A hollow cathode with a coaxial sparker was used in these experiments. This apparatus was essentially identical to that used by earlier experiments (Ref. 13). It did not, however, exhibit the same erosion characteristics. Use of the spectrometer provided the answer to this dilemma. Fig. 11 shows a typical spectrometer output when the spectrometer is adjusted to a strong line of the anode material. The second sharp high amplitude rise in the photomultiplier output is seen only when on an anode material line and is explainable on the basis of behavior of the pulse forming network. Earlier it was pointed out that the characteristics demonstrated in Fig. 7 would play an important part in the analysis of the experiments. Note that if the output resistance is too small, the initial current pulse is larger. Thus being naturally

inclined to get the most out of a given piece of equipment, the experimenter will tend to install the smallest resistance value that seems reasonable. He decides the value to use by looking at the shunt output. When the overshoot appears to be becoming excessive, the resistance value is made no smaller. Due to the scales involved, in order to see the first pulse of several thousand amps, one does not see this overshoot until it reaches at least the order of 100 amps. Unfortunately any overshoot at all is excessive. The anode becomes the cathode during the period of this reverse current. The cathode heating is extremely localized and results in very rapid erosion, which is the explanation of the second rise in spectrometer output of Fig. 11. Cathode, rather than anode, material is being vaporized.

It is obvious that one must build the apparatus with a tendency toward too high a resistance value so that the current shown in Fig. 7b is realized. Note that it is impossible to attain the idealized case of Fig. 7a since the arc does not constitute a constant impedance and also we are using a lumped parameter approximation to a transmission line.

With this potential pitfall recognized and with slightly excessive resistance, it was found that not only could copper vapor not be detected by the spectrometer, but no erosion could be detected either. There was only a fairly large discolored area. It was concluded that the pulse duration was not sufficient to cause erosion. As will be discussed later, this is not the

entire problem; there is also an effect due to cathode induced arc motion.

#### Larger bank with coaxial sparker cathode

The larger capacitors were purchased and an entirely new apparatus was built. This was set up initially with 2 micro-Henry inductances so as to get a 200 microsecond arc of 5000 amps in a 1 Ohm resistance when the capacitor bank was charged to 10,000 volts. This pulse forming network required an Ignitron to switch it as the capabilities of the previously used spark gap were exceeded. With the exception of the Ignitron trigger circuit, heater, etc., the circuit was essentially the same as was previously used. The same coaxial cathode sparker was used.

After considerable work with this apparatus, it was found from the spectrometer output that there was no anode material appearing in the arc. What is more, the anode surface appearance was very similar, though more discolored, to its appearance for the 40 microsecond, 5000 amp arc.

It appeared that there was still not enough energy to cause erosion.

The possibility of reducing the inductances to 1/2 micro-Henry so as to get a 100 microsecond pulse of 10,000 amps in a 1/2 Ohm resistance when the capacitor bank was charged to 10,000 volts was considered. This method of increasing current is very limited for one must also decrease the matching resistance according to  $Z_0 = \sqrt{L/C}$ . In order to get anything approaching a square pulse,

the line resistance must be much greater than the widely varying arc impedance. If the anode spot size and the anode fall were to remain roughly constant when the current doubled, one would expect the heat flux to double; at least one would expect a considerable increase. Calculations show (Fig. 5) that the time to vaporization is inversely proportional to the square of the heat flux. This is true for either the constant or variable property calculation. Thus, if the heat flux were doubled, the time required to vaporize the anode material would be cut by four, whereas the pulse duration would be cut by two. Thus, it was decided to try a 10,000 amp, 100 microsecond arc.

The apparatus was modified to do this. The result was much the same as for the 5000 amp, 200 microsecond arc.

#### Larger bank, effect of cathode configuration

During the tests with the cathode with the coaxial sparker (Fig. 12) at 10,000 amps, it was noted that the entire tungsten tip had a velvety appearance. As this cathode had been recently rebuilt, it was evident that the cathode attachment was moving extremely rapidly over the whole cathode tip. This is extremely important because of the cathode jet. When the jet emanates from the side of the cathode, it most certainly tends to cause the anode attachment area to move away from directly under the cathode in this direction. In all likelihood, the rapidly moving cathode attachment induces a rapid motion of the anode attachment within a radius centered directly below the cathode. This, of course,

would reduce the time averaged heat flux to an extremely low level. This explains the results of the experiments thus far described. This sort of motion for this cathode design is seen in the photographs in Fig. 3 of Ref. 15.

It was decided to try a pointed solid tungsten cathode (Fig. 13), the type cathode usually used in the High Temperature Laboratory. This particular electrode has had extensive use in low current steady state arcs with the conclusion that the arc should attach and remain at the tip. It was installed with an anode-cathode gap of slightly greater than . 7m, the maximum that would break down.

A lamp, mounted behind the cathode on a plexiglas bracket, was used to align the spectrometer (Fig. 14). The solid cathode first used had this lamp mount installed. The result for a 10,000 amp, 100 microsecond arc on the anode surface was a deep crater surrounded by a radial pattern of solidified copper which had been blown from the crater and an extremely dark deposit. There was, however, no copper vapor evident in the arc. The only possible conclusion is that the copper liquid was being blown away, probably by the cathode jet, as soon as it was formed and the surface never reached the vaporization temperature.

In order to align the spectrometer to more specific parts of the arc, the alignment light was removed and the spectrometer was aligned with a laser. With no changes to the arc configuration other than the removal of the plexiglas mount (Fig. 14), the anode

exhibited no erosion but only a large discolored area (Fig. 21-2) much the same as seen for the cathode with the coaxial sparker (Fig. 12 and 21-6).

It seemed obvious that the arc must be climbing the cathode so as to induce motion of the anode attachment area as described for the coaxial sparker cathode but that with the plexiglas mount installed this action was stopped. In order to see just how far the arc would climb the cathode, a brass cathode as shown in Fig. 13 was constructed. The arc left quite distinct tracks on this cathode. There were visible tracks as far as 3/8" from the tip. This type of behavior has been observed on newly ground tungsten cathodes in steady arcs so a tungsten cathode was run, in exactly the same physical situation, with a 100 amp steady arc for about two minutes. The arc attached in a normal manner at the cathode tip. When used again in the pulsed application, it climbed the cathode just as before. With the anode above the cathode, the arc climbed down on the cathode, thus eliminating the possibility of convection causing the motion.

The probable explanation for this behavior lies in a self-magnetic field driving the arc up the side of the cathode (Fig. 15). If the arc deviates from the tip slightly, it must have a bend in order to make the transition from the vertical direction of the column to the direction normal to the cathode surface. Because of this bend, the magnetic field of the column is into the paper at the attachment point. Thus,  $\vec{J} \times \vec{B}$  is in an upwards direction parallel to the cathode surface. Note that this assumes the current is carried symmetrically in the cathode and that the column size

and radius of bend into the cathode are small. The result is a force, roughly proportional to the square of the current, tending to move the cathode attachment point. This explains why, with the same cathode, the arc will stay at the tip for a steady state low current arc but climbs the cathode at an average vertical velocity of at least  $10^4$  cm/s for a 10,000 amp arc.

Numerous cathode designs have been tried to eliminate the cathode-induced anode attachment motion. Six of the cathode configurations which have been used are shown in Fig. 12, 13, 14, 16, 17, 18. The corresponding anodes are shown in Fig. 21. All anodes in Fig. 21 have been subjected to one 10,000 amp, 100 microsecond arc. Copper vapor was not seen for any of these anode-cathode combinations.

Fig. 21-2 shows the anode associated with the cathode of Fig. 13. The unsymmetry seen is due to a modified anode holder; if the holder had been the same as for the other shots, it would be more nearly symmetric. No erosion is seen, but rather only a discolored area.

Fig. 21-1 shows the anode associated with the cathode of Fig. 14. It shows a grossly melted crater surrounded by a dark radial pattern. Liquid copper is blown in a radial direction.

Fig. 21-5 shows the anode associated with the cathode of Fig. 16. It shows a similar pattern to that of Fig. 21-1 but is more colorful. The blackness of Fig. 21-1 may be attributable to plexiglas which is charred and deposited on the anode. The outer

diameter of the dark area is smaller than Fig. 21-1 which may be a result of the shield restricting radial velocity of the expanding gases.

Fig. 21-4 corresponds to the cathode of Fig. 17. This appears as a grossly melted region of about 0.5 cm diameter surrounded by a colorful somewhat less melted region. Craters are evident in both regions, but the radial pattern of melt flow is not seen as in Fig. 21-1 and 21-5.

Fig. 21-3 corresponds to the cathode of Fig. 18. This shows a dark center region, with tungsten deposited in the region of the center, surrounded by a clean cratered region, in turn surrounded by a radial flow of copper.

Fig. 21-6 corresponds to the cathode of Fig. 12, the same design as used by the study at General Dynamics. This shows a pattern similar to that of Fig. 21-2. The size of the center dark region is somewhat larger relative to the overall size of the discolored area than for Fig. 21-2.

### C. Results

The design of a cathode which will be useful in studying the anode of a high current arc presents something of a dilemma. If the cathode attachment is restricted to the tip, the cathode jet is directed toward the anode which, of course, influences the results. On the other hand, if the arc emanates from the side of the cathode, as it moves around it causes the anode attachment to move.

A cathode design (Fig. 19) is to be tried in an attempt to circumvent these problems. The idea is to make use of the self-magnetic field to drive the attachment into the throat of a hollow cathode. The impact of the cathode jet would then be taken to a great extent by the opposite wall while the region from which the arc emanates at the cathode is restricted to the area of the throat so that the cathode attachment motion should induce a minimum of anode attachment motion. Any impact of hot gas on the anode from thermal expansion should be minimized by allowing the gases to expand upwards. The smaller diameter center electrode may be used to help start the arc in either of two ways; it can be used as a sparker by applying a high voltage between it and the cathode, or it may be connected to the cathode by a resistance so that when the 10,000 volts are applied to the cathode, the gap will break down due to the pointed cathode but when appreciable current begins to flow the arc will transfer to the main cathode. This cathode is presently being constructed.

Two other possibilities exist for eliminating the cathode influence. One is to restrict the cathode attachment to the tip of a pointed cathode and to have a very large gap between the anode and cathode. This, of course, creates problems in starting the arc. This could be done by reconstructing the apparatus so that the first inductor in the Guillemin line is adjacent to the electrode and applying a pulse of 70  $\rightarrow$  100 KV of nanosecond duration. Another is to place an orifice below the cathode. If properly sized, it should cause a reverse flow towards the cathode that counteracts the effect of the cathode jet (Fig. 20).

#### IV. SUMMARY AND CONCLUSIONS

In order to have valid anode measurements, one must be extremely cautious to eliminate the influence of the cathode, both the impingement of the cathode jet on the anode and the motion of the anode attachment area induced by the cathode spot motion.

Without special care in cathode design, either the arc will move rapidly over a large area of the anode surface and yield extremely low heat fluxes; or the cathode jet will impinge on the anode surface which renders the results meaningless.

Several cathode designs have been tried and have given insight into the behavior of this particular arc. Further work with cathode design is expected to result in a cathode with which the undisturbed anode phenomena can be studied.

## REFERENCES

- [1] Cohen, M. I., "Melting of a Half-Space Subjected to a Constant Heat Input", J. of The Franklin Institute, Vol. 283, No. 4, April, 1967, p. 271.
- [2] Hashemi, H. T. and Sliepcevich, C. M., "A Numerical Method for Solving Two-Dimensional Problems of Heat Conduction with Change of Phase", Chemical Engineering Progress Symposium Series, Heat Transfer with Change of Phase, Vol. 63, No. 79, 1967, p. 34.
- [3] Hashemi, H. T., Ph.D. Thesis, University of Oklahoma, Norman (1965).
- [4] Douglas, Jim, Jr., "A Survey of Numerical Methods for Parabolic Differential Equations", Advances in Computers, Edited by Alt, F. L., Vol. 2, 1961, Academic Press, p. 1.
- [5] Hultgren, R., Orr, R. L., Anderson, P. D., and Kelly, K. K., Selected Values of Thermodynamic Properties of Metals and Alloys, John Wiley and Sons, Inc., 1963.
- [6] Thermophysical Properties Research Center, Purdue University, Touloukian, Y. S. and Ho, C. Y., Editors, Thermophysical Properties of Matter, Plenum Publishing Corp., 1970.
- [7] Smithells, J. C., Metals Reference Book, Fourth Edition, Butterworth, Inc., 1967.
- [8] Chou, T. S., "Anode Contraction Mechanism of High Intensity Arcs", Ph.D. Thesis, University of Minnesota, June, 1971.
- [9] Carslaw and Jaeger, Conduction of Heat in Solids, Oxford Press, 1959.
- [10] Glasoe, G. N. and Lebacqz, J. V., Pulse Generators, Dover Publications, Inc., 1965.
- [11] Metzger, G. and Vabre, J. P., Transmission Lines with Pulse Excitation, Academic Press, Inc., 1969.
- [12] Wilson, W. R., "High Current Arc Erosion of Electrical Contact Materials", Proceedings for Engineering Seminar on Electrical Contacts, June 25-29, 1956, Pennsylvania State University

- [13] Shih, K. T., "Electrode Erosion in High Current Arcs", March, 1970, Contract No. F 33615-67-C-1386, Project 7063.
- [14] Avseyevich, O. I., "Principles of Erosion During Pulsed Discharges", Physical Bases of Electric Spark Machining of Materials, Moscow, Izd-vo Nauka, 1966, p. 32-41.
- [15] Shih, K. T., "Investigation of Electrode Erosion in High Current Electric Arcs", Report for period from March 1 to March 31, 1969, Contract F 33615-67-C-1386.

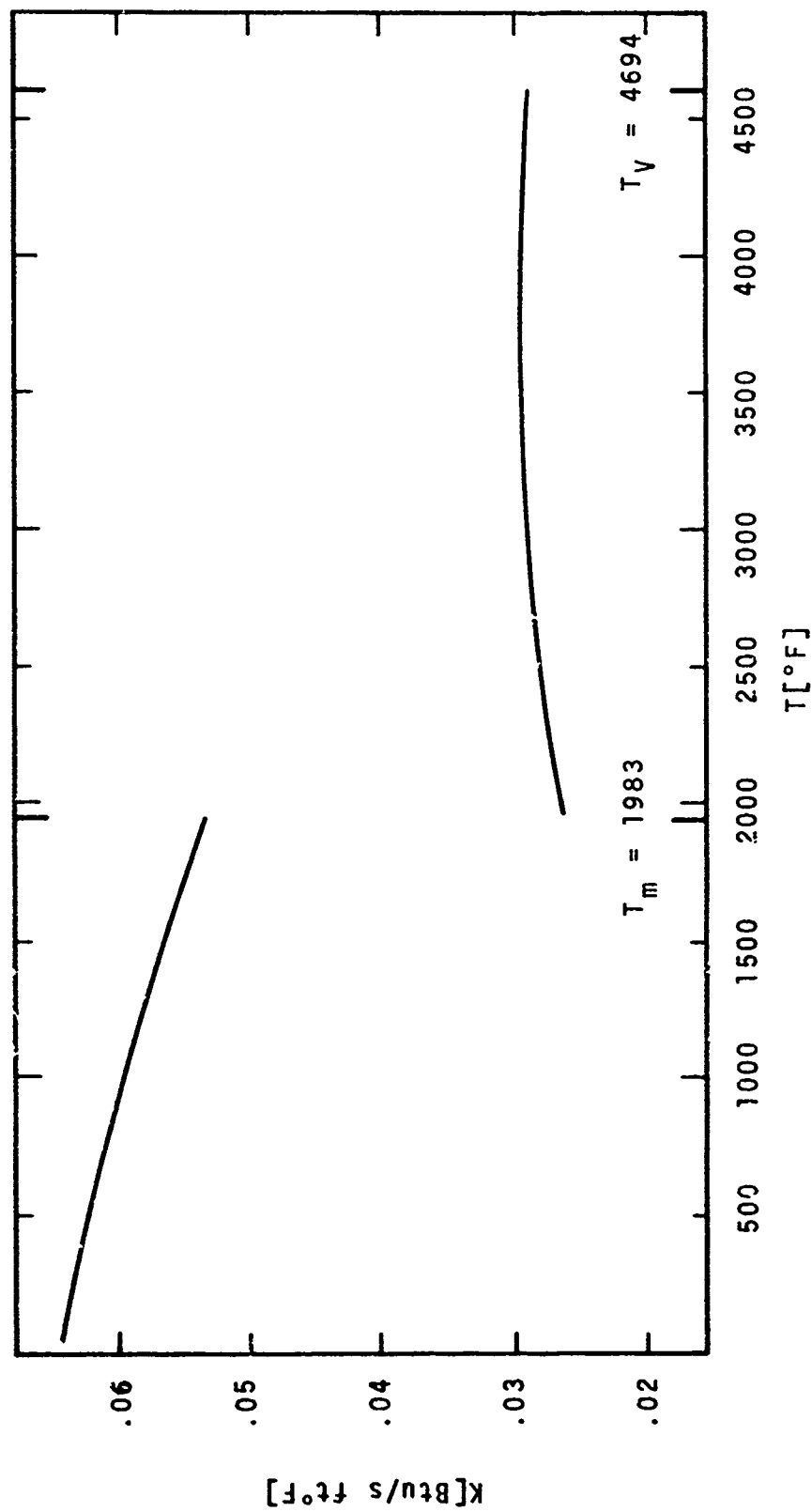


Fig. 1: Copper Thermal Conductivity

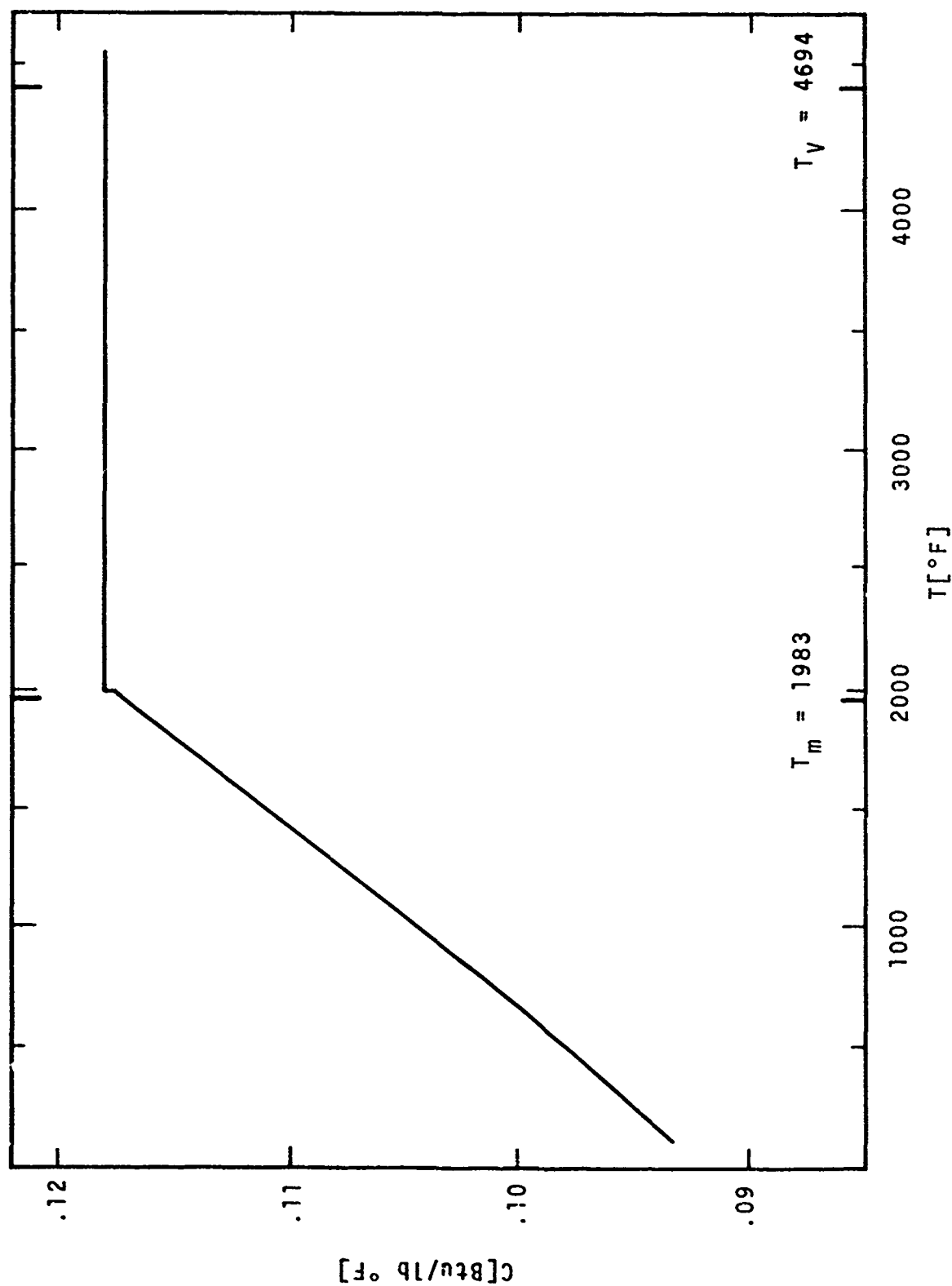


Fig. 2: Specific Heat of Copper

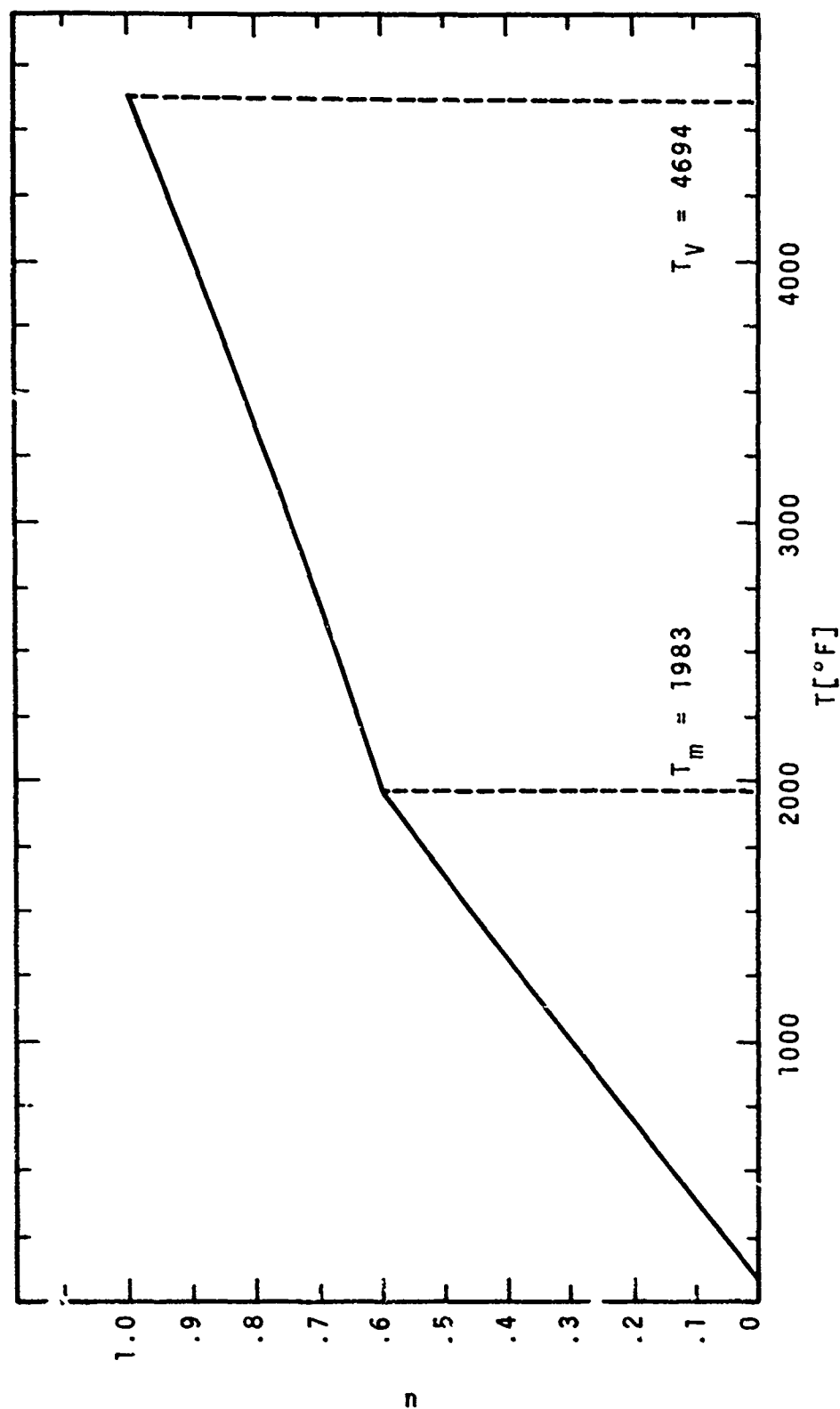


Fig. 3: Dimensionless Temperature ( $u$ ) for Copper

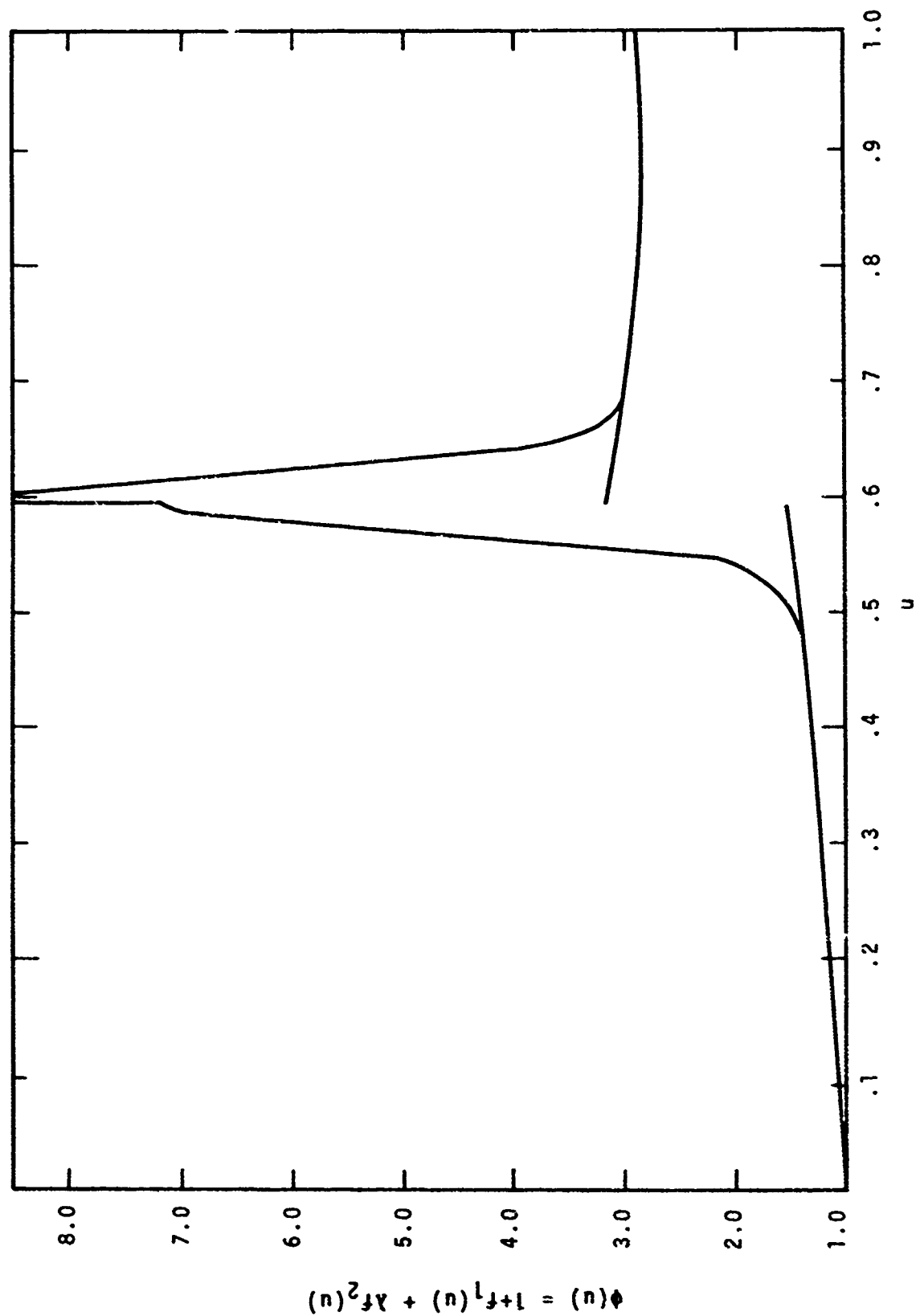


Fig. 4: Copper  $\phi(u)$ , Function Used in the Solution of Transient Conduction Equation (Eq. 6e)

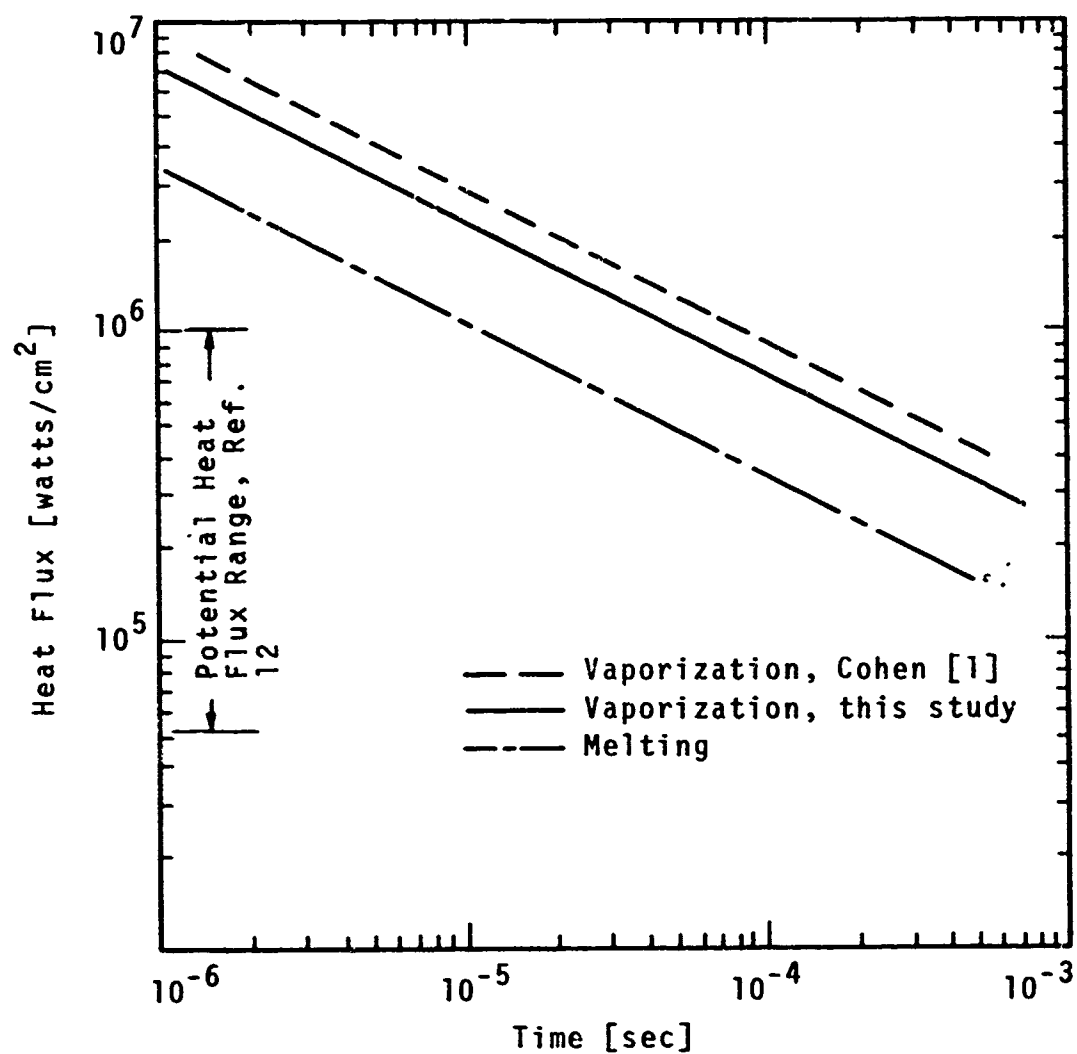


Fig. 5: Time to Melting and Vaporization for Copper

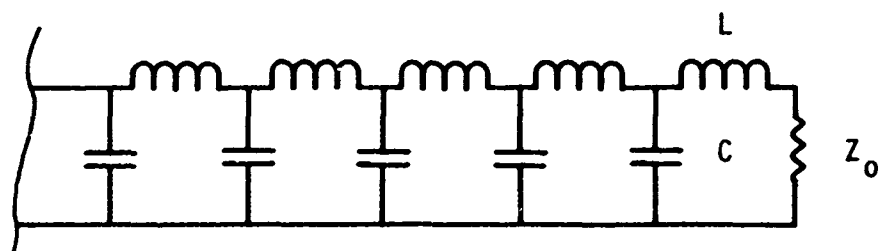


Fig. 6: Guillemin Network

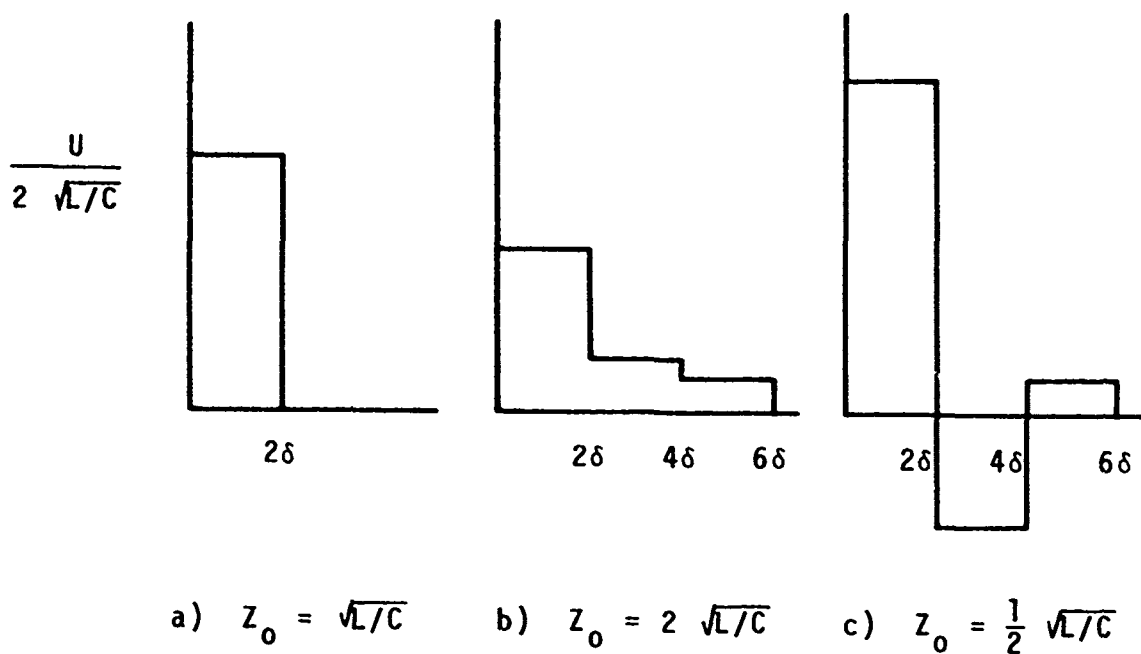


Fig. 7: Current for Guillemin Network  
Discharging into Resistive Loads

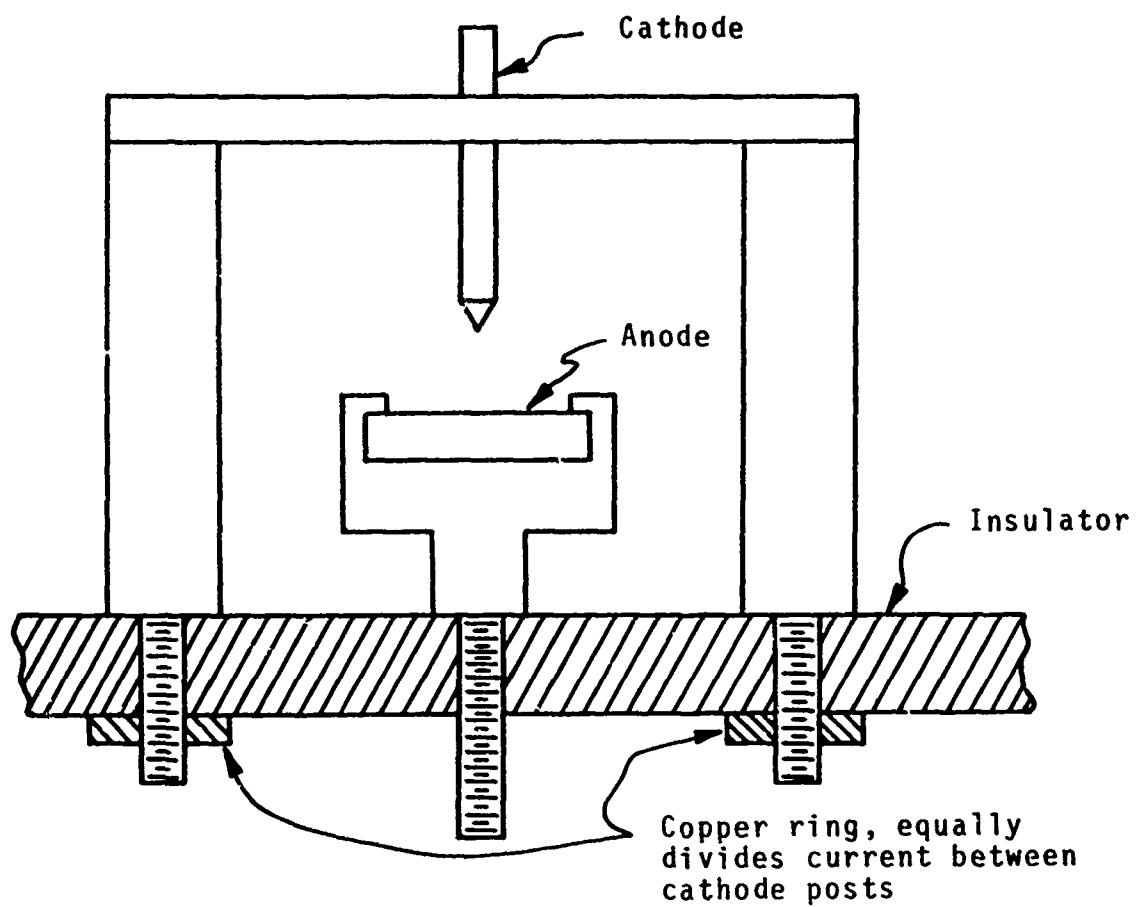


Fig. 8: Anode-Cathode Mounting  
for Pulsed Arc

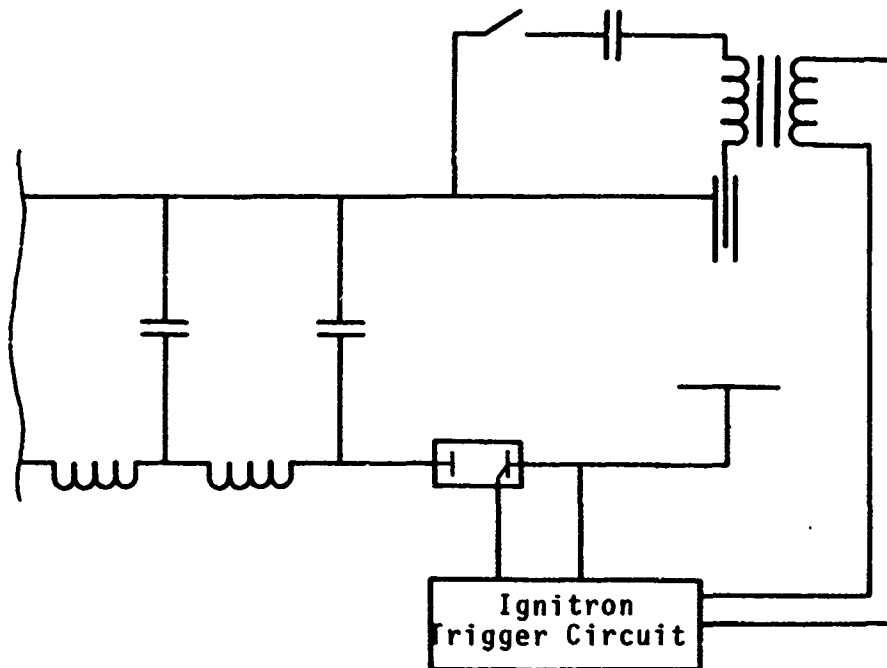


Fig. 9: Circuit with Cathode/Sparker

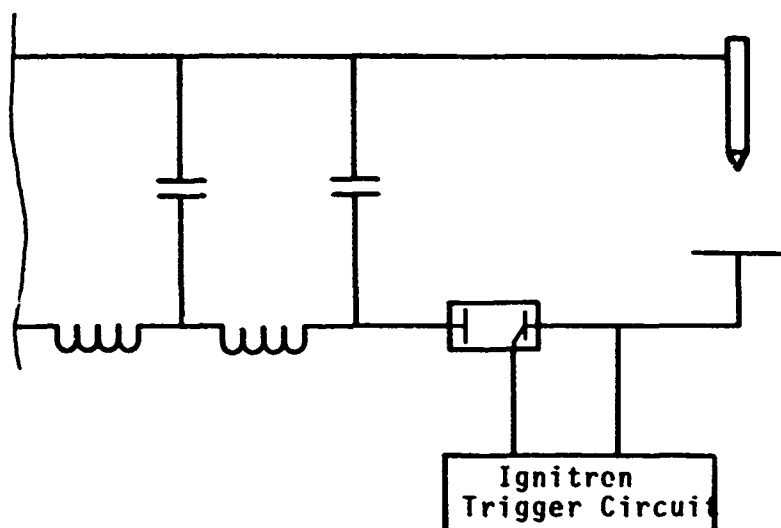
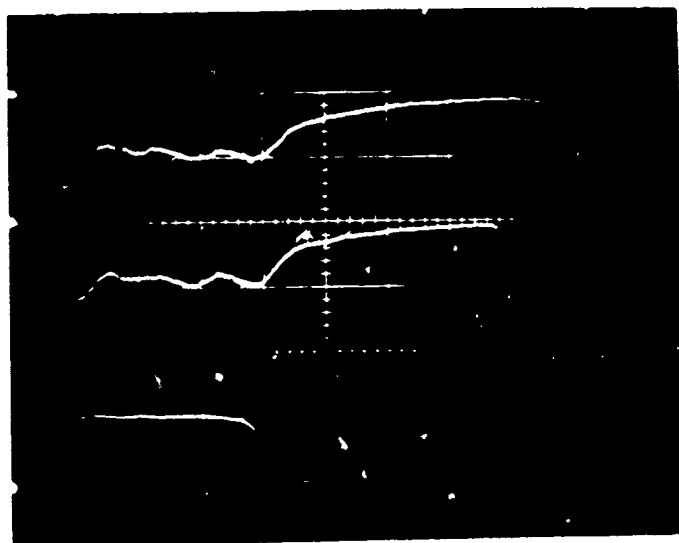


Fig. 10: Circuit with Solid Cathode



Reproduced from  
best available copy.

Fig. 11: Current and light emission ( $5218 \text{ \AA}$ )  
for  $\text{N}_2$  arc with copper anode; current  
4166 Amp/cm, light relative magnitude  
only; second firing shows current  
reversal

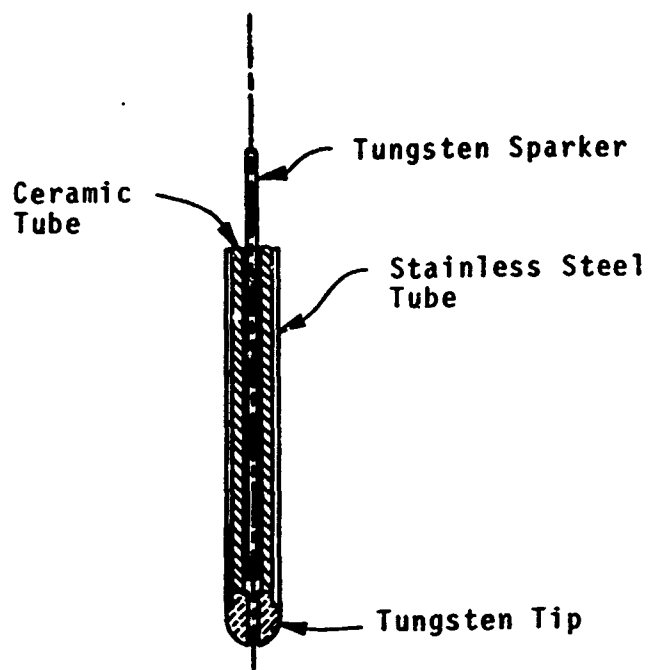


Fig. 12



Fig. 13

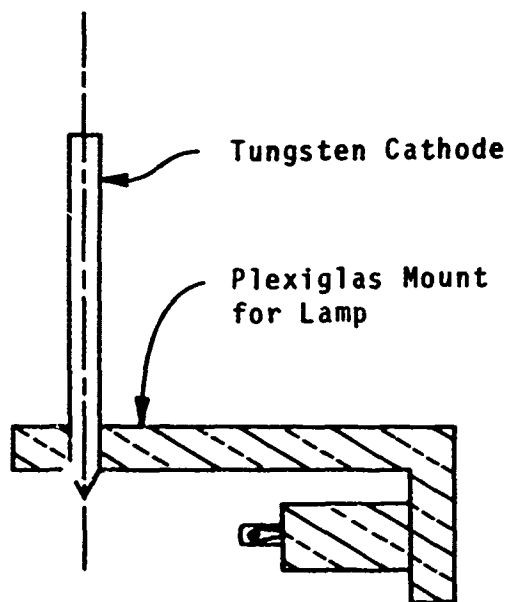


Fig. 14

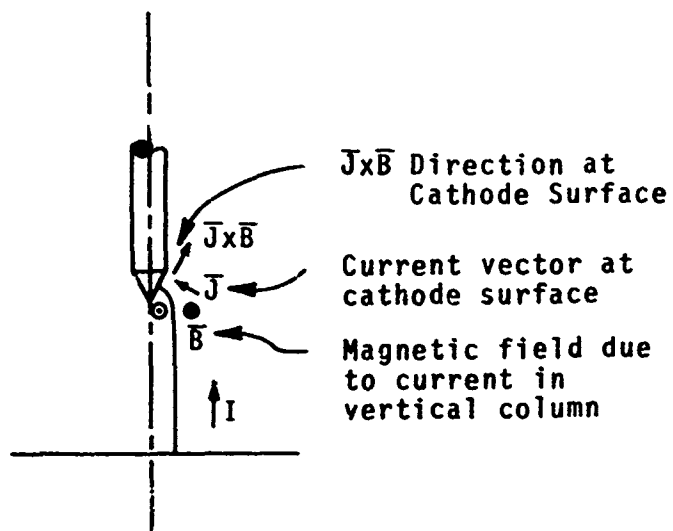


Fig. 15

### Various Cathode Arrangements

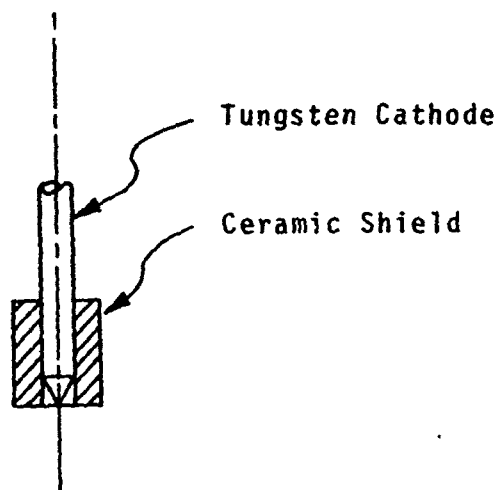


Fig. 16

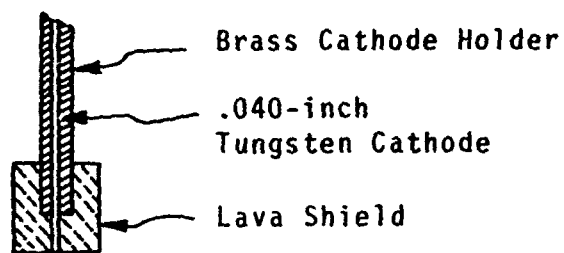


Fig. 17

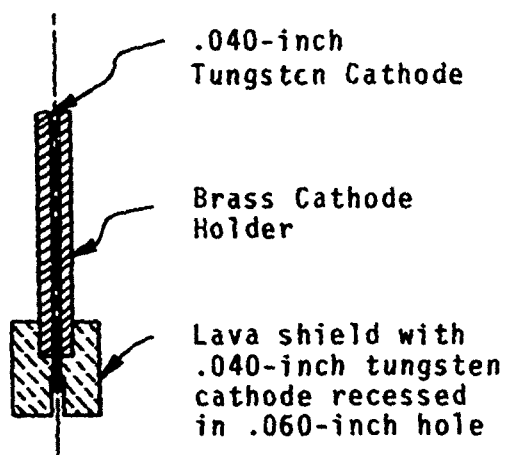


Fig. 18

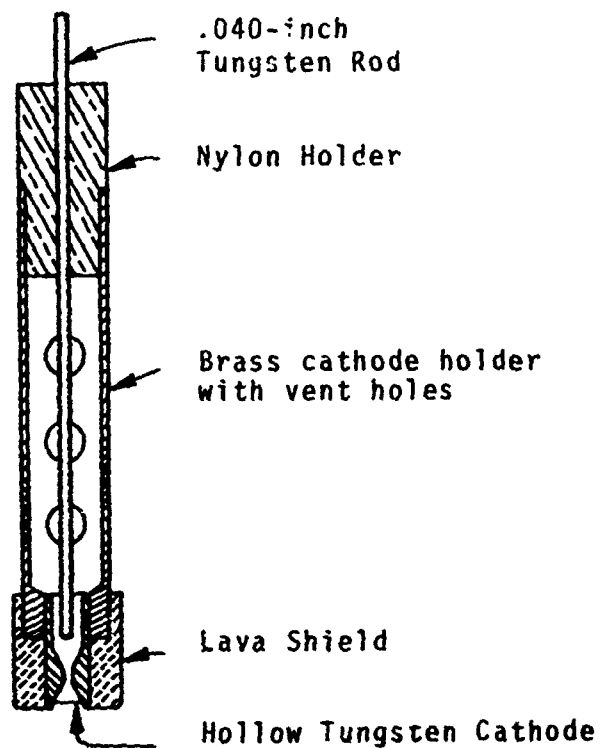


Fig. 19

### Various Cathode Arrangements

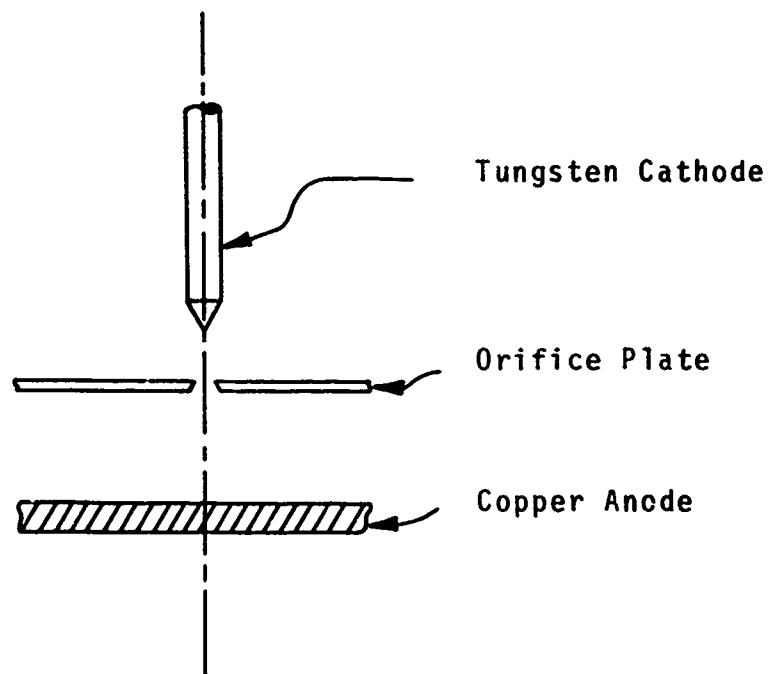


Fig. 20  
Cathode Design for Eliminating the Effect  
of the Cathode Jet on the Anode

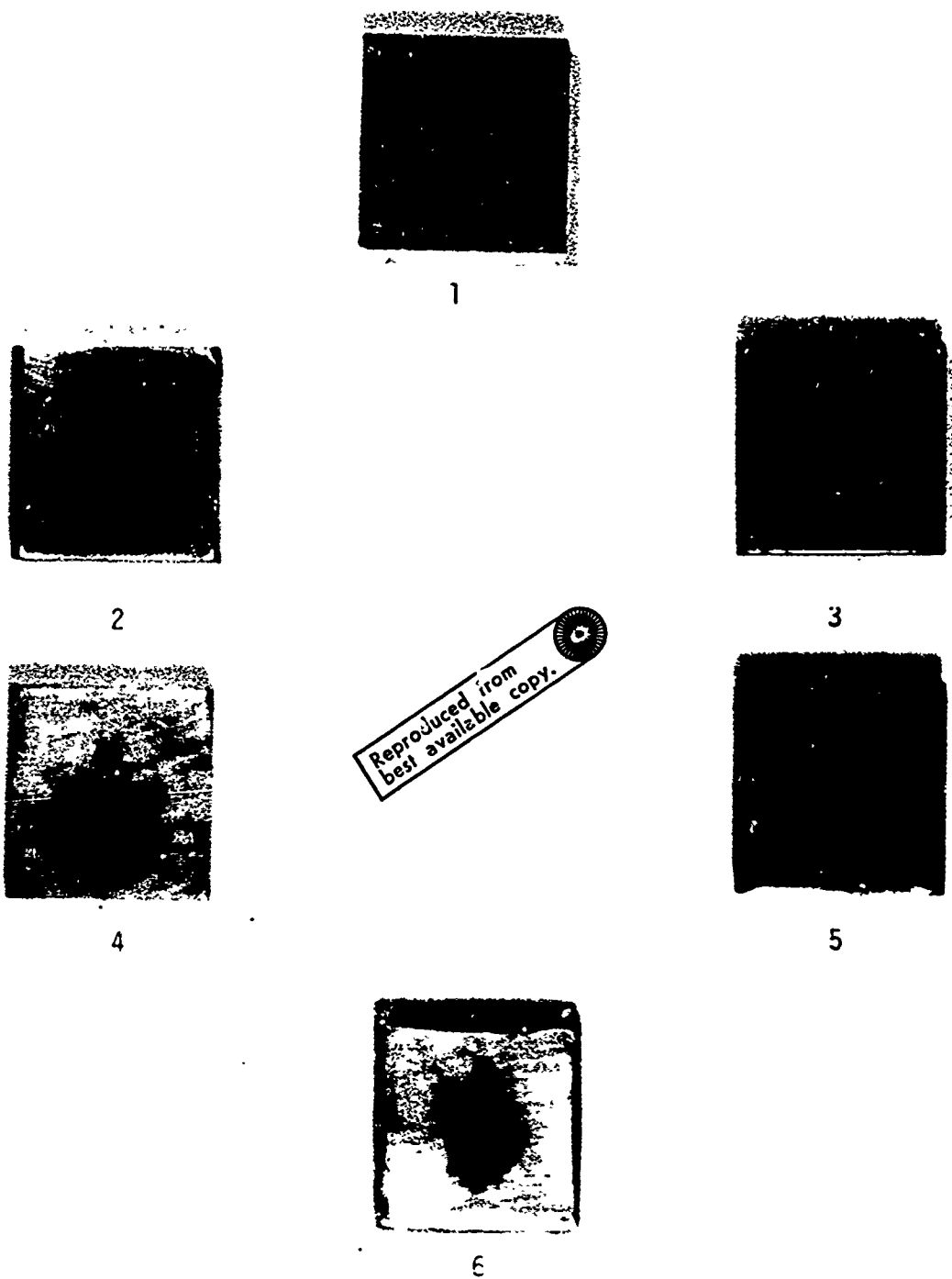


Fig. 21: Some Typical Anode  
Erosion Marks